Synthesis and structural characterization of the Ca_2MnReO_6 double perovskite

(Síntese e caracterização estrutural da dupla perovsquita Ca_2MnReO_6)

H. P. S. Corrêa[1], I. P. Cavalcante[1], D. O. Souza[2], E. Z. Santos[2], M. T. D. Orlando[2], H. Belich[2], F. J. Silva[2], E. F. Medeiro[2], J. M. Pires[2], J. J. Passamai[2], L. G. Martinez[3], J. L. Rossi[3]

[1]Universidade Federal de Mato Grosso do Sul, Campo Grande, MS

[2]Universidade Federal do Espírito Santo, Av. Fernando Ferrari 514, Vitória, ES 29075-910

[3]Instituto de Pesquisas Energéticas e Nucleares, IPEN-CNEN, Av. Prof. Lineu Prestes 2242, Cidade Universitária, S. Paulo, SP 05508-000

mtdorlando@gmail.com

Abstract

The $Ca_2Mn_1Re_1O_6$ double perovskite has been prepared in polycrystalline form by using the encapsulated quartz tube method. The partial oxygen pressure inside the quartz tube revealed this to be a crucial synthesis parameter for the production of a single structural phase sample. This parameter was controlled using the ratio between ReO_2 and ReO_3 content and the filling factor parameter (ratio between mass and total inner volume of the quartz tube). The morphology and chemical composition was investigated by scanning electron microscopy and energy dispersive X-ray spectroscopy. The crystal structure parameters were determined by analysis of the synchrotron high-resolution X-ray powder diffraction pattern. The analysis indicates that the sample is an ideal single-phase compound with a monoclinic crystal structure (space group $P2_1/n$) with a = 5.44445(2) Å; b = 5.63957(3) Å; c = 7.77524(3) Å; and β = 90.18(1)º. Computer simulations were performed considering two cation valence configurations, namely, (i) $Mn^{2+}Re^{6+}$ or (ii) $Mn^{3+}Re^{5+}$, for the $Ca_2Mn_1Re_1O_6$ compound. XANES analysis measurements indicated +2.3 for the average valence of Mn (a mixture of Mn^{2+} and Mn^{3+}) and +5.7 for the effective valence of Re (an intermediate valence between Re^{4+} (ReO_2) and Re^{6+} (ReO_3)). As a summary, we concluded there is a mixed valence configuration for Mn and Re in $Ca_2Mn_1Re_1O_6$, taken into account the oxygen content of 6.0±0.1 .

Keywords: double perovskite, X-ray diffraction, lattice parameters.

Resumo

A dupla perovsquita Ca_2MnReO_6 na forma policristalina foi preparada utilizando o método do tubo de quartzo encapsulado. A pressão parcial de oxigênio dentro do tubo de quartzo mostrou-se ser um parâmetro crucial para a produção de uma amostra estrutural monofásica. Esse parâmetro foi controlado usando a relação entre o conteúdo dos precursores ReO_2 e ReO_3 e o parâmetro fator de preenchimento (razão entre a massa e o volume interno total do tubo de quartzo). A morfologia e a composição química foi investigada através da microscopia eletrônica de varredura e espectroscopia de energia dispersiva de raios X . Os parâmetros de estrutura cristalina foram determinados através da análise do padrão de difração tomado com luz síncrotron de alta resolução. Finalmente, os parâmetros cristalinos foram comparados com os resultados oriundos dos cálculos de Bond-Valence Method oriundos do programa SPuDS. Como resumo, a análise indicou que a amostra é um composto monofásico com uma estrutura cristalina monoclínica (grupo espacial P21/c) com a = 5,44445(2) Å; b = 5,63957(3) Å; c = 7,77524(3) Å; and β = 90,18(1)º.

Palavras-chave: *perovsquita dupla, difração de raios X, parâmetros de rede.*

INTRODUCTION

The ordered double perovskite oxides, whose general formula is $A_2B'B''O_6$, were first proposed by Longo and Ward [1] in 1961. According to those authors, A is an alkaline-earth divalent cation, B' and B'' are transition-metals and present an octahedral coordination with the anion O^{2-} [2]. This type of compound exhibits magnetic and electronic properties related to the strong interplay between structure, charge and spin ordering [3], which is the subject of nano-spintronic studies. Spintronics is an emerging field of science and technology that will most likely have a significant impact on the future of all aspects of electronics [4-6]. Moreover, spintronics is the next step towards the new technology of spin-based quantum computing and quantum information processing [7-9], voltage controlled spintronic devices for logical applications [10] and semiconductor devices [11,12].

The early discovery of large low-field room-temperature magnetoresistance in these compounds (mainly in half-metallic Sr_2FeMoO_6, described by Kobayashi in 1998

[13]) stimulated interest in the study of the properties of ordered double perovskites, in the context of their potential application in the field of spin electronics [14-17]. The focus of these studies was to characterize their magnetic and electronic properties as well as their crystallographic structures. Among them, the $A_2M\mathrm{ReO}_6$ series (namely Re-based ordered double perovskites), with A = Ba, Sr, Ca and M = Cr, Fe, Mn, shows a wide variety of magnetic and electronic properties. Concerning the magnetic state, the majority of the compounds reveal ferromagnetic behavior with the coupling of the divalent magnetic M ion to Re [18].

The ideal structure of the double perovskites is based on the adapted tolerance factor t of the single perovskite [19]. In general, for double perovskites $A_2B'B''O_6$, the tolerance factor can be written as

$$t = \frac{r_A + r_0}{\sqrt{2}\left(\frac{r_{B'}}{2} + \frac{r_{B''}}{2} + r_O\right)} \qquad (A)$$

where r_A, r_B and $r_{B''}$ are the ionic radii of the respective ions and r_O is the ionic radius of oxygen. The closer to $t = 1$, the more the structure corresponds to ideal cubic. Therefore, except in rare cases, one can consider the following rule for the double perovskite family: for $1.05 > t > 1.00$ a cubic structure is adopted within the $Fm\bar{3}m$ space group; for $1.00 > t > 0.97$ the most likely structure corresponds to the I 4/m tetragonal space group and if $t < 0.97$ the compound becomes either monoclinic ($P2_1/n$) or orthorombic [20]. Philipp *et al.* [18] reached a similar conclusion by studying the CrW-based series. Lufaso *et al.* [19] reported that roughly 70% of all ordered double perovskites undergo octahedral tilting distortions. By considering 11 possible distinct types of octahedral tilting, it was shown that five tilted systems accounted for ~97% of the reported structures. The five dominant tilted systems reported, namely $Fm\bar{3}m$ ($a^oa^oa^o$), *I 4/m* ($a^oa^oc^-$), $R\bar{3}$ ($a^-a^-a^-$), *I* 2/*m* ($a^ob^-b^-$) and *P* $2_1/n$ ($a^-a^-b^+$), as well as two additional tilted systems, $Pn\bar{3}m$ ($a^+a^+a^+$) and *P* 4/*mnc* ($a^oa^oc^+$), can be simulated using the *SPuDS* (Structure Prediction Diagnostic Software) [21].

Several reports like the ones by Philipp *et al.* [16] and Popov *et al.* [22] have studied the correlation between the *A*-site cation size and the properties of the double perovskites. Granado *et al.* [23] have concentrated on the spin-orbital manifestation of Re ion and its influence on the electronic properties of the Ca_2FeReO_6 compound. Herrero-Martín *et al.* [24] studied the X-ray absorption of the FeRe-base double perovskites series employing the most recent theoretical calculations in order to explain the magnetic and electronic results. Sikora *et al.* [25], employing X-ray magnetic circular dichroism at the Re $L_{2,3}$ edges, observed a considerable orbital magnetic moment, which implies an unquenched Re orbital moment, despite its octahedral coordination [26], in the similar series of FeRe-based double perovskites made by Herrero-Martín [24]. Finally, Serrate *et al.* [20] published a large topical review showing the importance of these materials for spintronic devices and that the physics involved in these compounds is more complex and rich than expected.

This work was proposed by taking into account a scenario which the magnetic and electronics properties of the $Ca_2Mn_1Re_1O_6$ double perovskite present a strong correlation with structural order. The main goal was to investigate the synthesis and crystal structure of the monophasic compound $Ca_2Mn_1Re_1O_6$.

EXPERIMENTAL DETAILS

$Ca_2Mn_1Re_1O_6$ double perovskite oxide was synthesized from CaO, MnO_2, ReO_2 and ReO_3. The calcium oxide CaO was prepared by decomposition of $CaCO_3$ (Alfa Aesar reagent, 99.9965%) first at 950 °C for 24 h in dynamic vacuum and then at 1100 °C for 3 h under a flux of oxygen. The CaO removed from the furnace was immediately placed into a dry box. The MnO_2 was used as purchased (Alfa Aesar, puratronic, 99.999%). Both ReO_2 (Aldrich, 99.9%) and ReO_3 (Aldrich, 99.9%) powders were also used as purchased. The mixture of CaO, MnO_2, ReO_2 and ReO_3 powders in the 2:1:0.9:0.1 stoichiometric ratio was ground and pelletized inside a dry glove box filled with Argon gas. This mixture of starting materials was wrapped in gold foil and sealed in an evacuated (10^{-2} torr) quartz tube. Care was taken not to overheat the samples while sealing the quartz tubes under vacuum, due to the high vapor pressure of ReO_3 at relatively low temperatures. The 0.9:0.1 ratio between ReO_2 and ReO_3 was used in order to obtain a partial oxygen pressure inside the quartz tube at high temperatures during the first thermal treatment. The ratio between sample mass and quartz tube inner volume was defined as the filling factor *ff*. The required filling factor was estimated to be $ff \cong 0.12 g/cm^3$ in order to obtain 3 bar of oxygen partial pressure during the first thermal treatment at high temperature. This partial oxygen pressure inside the quartz tube revealed it to be a crucial synthesis parameter for the production of a single structural phase sample. The oxygen pressure inside the quartz tube after the first thermal treatment at room temperature was 750 mmHg and it was measured by a home made pressure setup with accuracy of 20 mmHg. The oxygen stoichiometry of the sample was evaluated by taking into account the mass variation of the oxide mixture before and after the thermal treatment by an analytical balance (Sartorius, Model TE2145, 0.0001g accuracy). The quartz tube was placed inside a gas pressure furnace filled with argon gas at 20 bar pressure in order to avoid quartz tube leakage during the thermal treatment. The sample was sintered for a total time of 154 h at 985 °C with two intermediate grinding steps then finally cooled down slowly in the furnace.

The morphology of the particles and their chemical composition were determined using a scanning electron microscope (SEM) together with an X-ray energy dispersive spectrometer (EDS). The SEM observations were carried out at magnifications up to x8,000. The electron beam energy was 20 keV, and probe current of the order of 25 μA. Fig. 1 shows the morphology of the particles present in the

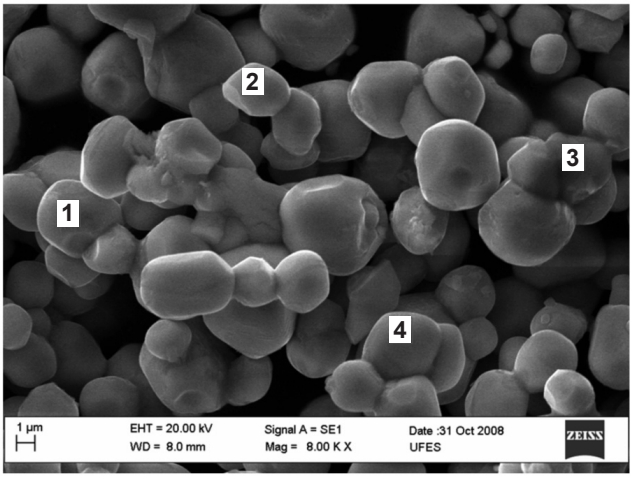

Figure 1: Back scattered electron image of a $Ca_2Mn_1Re_1O_6$ sample carried out using a Zeiss Evo 40. The numbers (1, 2, 3 and 4) represent regions where the energy dispersive X-ray spectroscopy (EDS) microanalysis was performed.

[Figura 1: Imagem da amostra Ca_2MnReO_6 utilizando elétrons retroespalhados usando um Zeiss EVO 40. Os números (1, 2, 3, e 4) representam regiões onde a microanálise por espectroscopia de raios X dispersiva (EDS) foi executada.]

$Ca_2Mn_1Re_1O_6$ and the regions of EDS microanalysis.

The high-resolution X-ray powder diffraction measurement was performed at the D10b-XPD beamline of the Brazilian Synchrotron Light Laboratory (LNLS), at Campinas city, using a wavelength λ = 1.54044 Å, at ambient pressure. A Ge(111) analyzer crystal was placed in a goniometer attached to the 2θ arm, and a scintillation

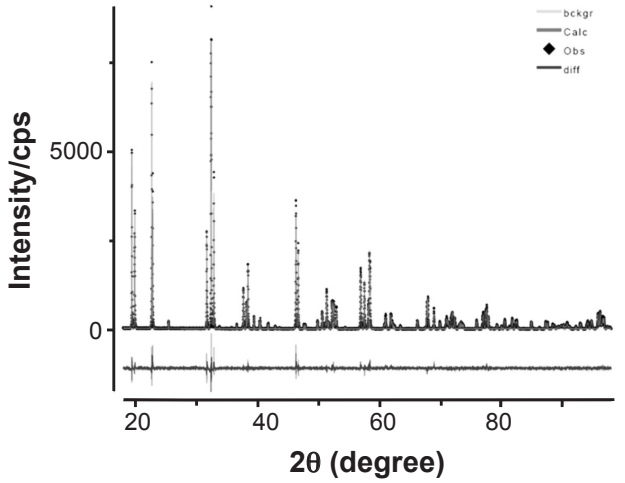

Figure 2: Observed (symbols - ◆), calculated (red line), background fitted (green line) and difference (bottom blue line) X-ray powder diffraction profile of sample Ca_2MnReO_6, taken with energy 8048 eV. The goodness-of-fit factors are R_{wp} = 0.1135, R_p = 0.0914, χ^2 = 2.568 and R_F^2 = 0.0549.

[Figura 2: Observado (símbolo -◆), calculado (linha vermelha), linha de fundo ajustada (linha verde) e diferença (linha de fundo azul). Padrão de difração de raios X de pó da amostra Ca_2MnReO_6 tomado na energia 8048 eV. Os fatores da qualidade do ajuste foram R_{wp} = 0,1135, R_p = 0,0914,χ^2 = 2,568 e R_F^2 = 0,0549.]

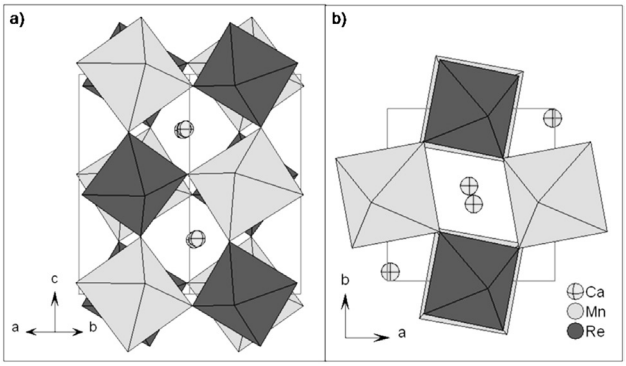

Figure 3: Schematic structure of Ca_2MnReO_6 (a) View of the unit cell along the crystallographic (110) direction corresponding to a pseudocubic a or b axis. The dark grey octahedra represent ReO_6 and the light grey octahedra represent MnO_6 ; opposite rotations of the octahedra along the viewing direction can be seen. (b) View along the crystallographic (001) direction showing in-phase rotations.

[Figura 3: Estrutura esquemática do Ca_2MnReO_6. (a) Vista de célula unitária ao longo da direção cristalográfica (110) que corresponde a um pseudocubico eixo a ou b. O octaedro cinza escuro representa o ReO_6 e o octaedro cinza claro representa o MnO_6; rotações opostas dos octaedros ao longo da direção podem ser vistas. (b) Vista ao longo da direção cristalográfica (001) mostrando as rotações em fase.]

detector was used. The Rietveld refinement was performed using the GSAS+EXPGUI suite [27, 28]. The sample of double perovskite studied showed 100% of the desired phase Ca_2MnReO_6. Observed, calculated, and difference profiles are shown in Fig. 2, and the structure is drawn in Fig. 3 (a) and (b). The structure reported by Kato *et al*. [17] was used as the initial model for the refinement. The peak profile function was modeled using a convolution of the Thompson-Cox-Hastings pseudo-Voigt (pV-TCH) function [29] with the asymmetry correction described by Finger et al. [30], to account for the asymmetry due to the beam axial divergence. In order to account for the anisotropy in the half width of the reflections, the bi-dimensional model described by Larson and Von Dreele [27] was used to account for the crystallite size and, for anisotropic strain, the model described by Stephens [31]. The value of the tolerance factor *t* was calculated using the bond valence parameters as obtained using the *SPuDS* simulation software [21]. *SPuDS* generates structures using computational tools for hypothetical compositions of those compounds where structural data are not available.

The local ReO_6 and MnO_6 octahedral oxygen coordination was investigated by X-ray absorption near edge (XANES) using the D08B – XAFS2 beamline. The measurements were recorded three times at Re L_{III}-edge (10.535 keV) and at Mn K-edge (6.540 keV) in transmission mode at room temperature. Si (111) channel-cut (2*d* = 6.271 Å) crystal produced a monochromatic beam in focus with 500 µm diameter at 0.005 mrad (0.3 eV) resolution @ 7keV. The energy calibration was carried out using the first inflection point of the XANES spectrum of Mn (K-edge = 6.540 keV) and Pt (L_{III}-edge = 11.564 keV) foils as references.

RESULTS AND DISCUSSIONS

Oxygen stoichiometry

The CaO (99.99%), MnO_2 (99.999%), ReO_2 (Aldrich, 99.9%) and ReO_3 (Aldrich, 99.9%) powders were mixed in the 2:1:0.9:0.1 stoichiometric ratio. The stoichiometric equation is described below.

$$2.00x(CaO) + 1.00x(MnO_2) + 0.90x(ReO_2) + 0.10x(ReO_3) \Leftrightarrow Ca_2Mn_1Re_1O_6 + 0.05x(O_2)$$

This mixture of starting materials was wrapped in gold foil and sealed in an evacuated (10^{-2} torr) quartz tube. The total mass of oxide mixture and gold foil together was measured by an analytical balance (0.0001 g accuracy) before and after the thermal treatment. The oxygen stoichiometry was determined by taking into account the mass variation and the residual oxygen pressure measured in the quartz tube at room temparature after each thermal treatment, and also considering the analytical balance accuracy (0.0001 g) and the pressure measurement setup accuracy (20 mmHg). The final oxygen stoichiometry was 6.0±0.1.

Scanning electron microscopy

A visual inspection of the SEM image (Fig. 1) indicates that the particles are almost equiaxial with sizes varying between 1 and 3 μm. The EDS elemental analysis of the particle center (number 1 in the image) detected the elements Ca, Mn, Re and O. The same elements were found at the other points (2, 3 and 4). No other elements were found at any of the points (1, 2, 3 and 4), taking into account the accuracy of EDS microanalysis system. The $Ca_2Mn_1Re_1$ stoichiometry was confirmed by EDS. The backscattered electron image indicates a chemically homogeneus composition present at the center and on the periphery of the particles.

X-ray powder diffraction

A monoclinic structure (space group $P\ 2_1/n$) was used to analyze the diffraction pattern. No secondary phases or impurities were observed in the diffractogram. The sample appeared to be homogeneous, with high crystalline quality, with no sign of anisotropic strain. The oxygen anions were constrained in order that they all have the same isotropic atomic displacement parameter. Refinements of occupancy at *B* and *B*' sites indicate that the ordering of Mn and Re atoms is 98%, therefore cationic disorder into the Re/Mn sites is ≅ 2%. Therefore, for the present discussion of crystal structure, the *B*-site disorder will not be considered. The monoclinic structure is the preferred structure for rock-salt type ordering of double perovskites with *t* values lower than 0.97. A major consequence of the distortion is that the Mn—O—Re angle is considerably lower than 180º (in the present case equal ~149°. The overall fitting quality is satisfactory. The refined structural parameters are given in Table I and the relevant bond-lengths and angles are given in Table II.

The Rietveld fit results of the atomic positions in Table I show that Mn cations occupy the 2d position, Re the 2c position and the Ca cation and three oxygen anions occupy different 4e positions. The monoclinic structure with tilts of the octahedra is drawn in Figs. 3a and 3b. According to Glazer's notation, there is an $a^-a^-b^+$ configuration along the pseudo-cubic axes [32]. A positive superscript would denote the neighboring octahedra tilt in the same direction (in-phase) and a negative superscript implies in tilts of neighboring octahedral in opposite directions (out of phase). The view in Fig. 3a along the pseudo-cubic *a* (or *b*) axis shows octahedra rotations with opposite sign and Fig. 3b

Table I - Rietveld fit results of the lattice and atomic parameters of sample Ca_2MnReO_6. The errors represent the standard deviation (statistical only).
[Tabela I - Resultados de refinamentos de Rietveld da rede e dos parâmetros atômicos da amostra Ca_2MnReO_6. Os erros representam o desvio padrão (somente estatístico).]

$P2_1In$	a = 5.44445(2) Å	b = 5.63957(3) Å	c = 7.77524(3) Å	β = 90.18(1)º
Atom	x	y	z	U_{iso}(Å²)	Occup.
Ca	0.4860(5)	0.55429(31)	0.25302(28)	0.0052(5)	1
Mn1	1/2	0	1/2	0.0086(5)	0.977
Re1	1/2	0	0	0.0030(2)	0.977
Re2	1/2	0	1/2	0.0086(5)	0.023
Mn2	1/2	0	0	0.0030(2)	0.023
O1	0.3155(11)	0.2861(11)	0.0496(9)	0.0044(12)	1
O2	0.2138(12)	0.8045(12)	0.0490(9)	0.0044(12)	1
O3	0.5952(10)	0.0407(12)	0.2425(7)	0.00441(12)	1

shows the view along the crystallographic *c* axis with the in-phase rotation of the octahedra

The prediction of crystal structure and the value of *t*

Table II - Length and bond angles of Ca_2MnReO_6 The errors represent one standard deviation and are statistical only.
[Tabela II - Comprimentos e ângulos de ligação do Ca_2MnReO_6. Os erros representam o desvio padrão e são estatísticos somente.]

MnO_6		ReO_6	
Mn1-O1(X2)	2.133(6)Å	RE1 - O1(X2)	1.940(6)Å
Mn1-O2(X2)	2.109(7)Å	RE1 - O2(X2)	1.947(7)Å
Mn1-O3(X2)	2.082(5)Å	RE1 - O3(X2)	1.967(5)Å
<Mn-O>	2.108(3)Å	<RE1 - O>	1.951(3)Å
-Mn-O-Re	-Mn-O1-Re	148.4(3)º	
	-Mn-O2-Re	150.2(4)º	
	-Mn-O3-Re	147.5(3)º	

calculated using the bond valence parameters were obtained using the *SPuDS* simulation software. The *SPuDS* output file contains a complete crystallographic description of the compound, including the space group, lattice parameters, atomic coordinates, bond-valence sums, individual bond valences and distances, tolerance factor, unit-cell volume, octahedral tilt angles, *B*—*X*—B' bond angles and global instability. To calculate bond-valence sums the program uses the Brown model [33, 34]. This model assumes that the valence of a given cation is shared between the chemical bonds of the first coordination sphere. It defines a phenomenological relationship between the formal valence of a bond and the corresponding bond lengths.

In this case, the metals Mn and Re can have two possible configurations: (i) $Mn^{2+}Re^{6+}$ and (ii) $Mn^{3+}Re^{5+}$. Therefore, two estimates of crystal structure by *SPuDs* for $Ca_2Mn^{2+}Re^{6+}O_6$ and $Ca_2Mn^{3+}Re^{5+}O_6$ perovskites (space group $P\,2_1/n$) having tilt system $a^-a^-b^+$ are given in Table III.

Comparing the crystal parameters carried out from the Rietveld refinement (Table I) with those evaluated by SPuDs (Table III), one observes that the Rietveld refinement results are between the high value represented by $Ca_2Mn^{2+}Re^{6+}O_6$ and the low value presented by $Ca_2Mn^{3+}Re^{5+}O_6$. The tolerance factor *t* evaluated for $Ca_2Mn^{3+}Re^{5+}O_6$ is higher than that for $Ca_2Mn^{2+}Re^{6+}O_6$. However, both are lower than 0.97, which is in agreement with the $P\,2_1/n$ monoclinic symmetry. The evaluated atomic positions of the Ca and O 4e sites are closer to the Rietveld refinement results.

Table III - SPuDS-predicte lattice parameters, atomic positions with tolerance factors t, lengths and angles bond for $Ca_2Mn^{2+}Re^{6+}O_6$ and $Ca_2Mn^{3+}Re^{5+}O_6$ perovskites (space group) having tilt system $a^-a^-b^+$.
[Tabela III - SPuDS-parâmetros previstos de rede, posições atômicas com fator de tolerância t, comprimentos e ângulos de ligação para as perovsquitas $Ca_2Mn^{2+}Re^{6+}O_6$ e $Ca_2Mn^{3+}Re^{5+}O_6$ (grupo espacial P21/n) apresentando um sistema torcido $a^-a^-b^+$.]

The b-siet cation listed first in the formula is located at (0,1/2, 0) and the second is at (1/2, 0, 0)

Formula	a(Å)	b(Å)	c(Å)	β(º)	t
$Ca_2Mn^{2+}Re^{6+}O_6$	5.4714	5.7352	7.9095	89.95	0.897
$Ca_2Mn^{3+}Re^{5+}O_6$	5.3850	5.5141	7.7031	89.99	0.943

Formula	Ca x	Ca y	Ca z	O1 x	O1 y	O1 z
$Ca_2Mn^{2+}Re^{6+}O_6$	0.4740	0.5735	0.2480	0.3226	0.2847	0.0555
$Ca_2Mn^{3+}Re^{5+}O_6$	0.4883	0.5372	0.2495	0.2950	0.2814	0.0389

Formula	O2 x	O2 y	O2 z	O3 x	O3 y	O3 z
$Ca_2Mn^{2+}Re^{6+}O_6$	0.2117	0.8161	0.0554	0.6109	-0.0209	0.2336
$Ca_2Mn^{3+}Re^{5+}O_6$	0.2171	0.7929	0.0389	0.5779	-0.3113	0.2441

Formula	Mn1-O1	Mn1-O2	Mn1-O3	Re1-O1	Re1-O2	Re1-O3
$Ca_2Mn^{2+}Re^{6+}O_6$	2.1978	2.1952	2.1964	1.9501	1.9479	1.9479
$Ca_2Mn^{3+}Re^{5+}O_6$	2.0166	2.0163	2.0165	1.9276	1.9273	1.9274

Formula	∠Mn-O1-Re	∠Mn-O2-Re	∠Mn-O3-Re
$Ca_2Mn^{2+}Re^{6+}O_6$	145.61	146.06	145.14
$Ca_2Mn^{3+}Re^{5+}O_6$	155.39	155.48	155.16

Moreover, by comparing Table II and Table III we observe that the angle Mn-O-Re and the bond distances Mn-O and Re-O have values between the evaluated limits defined by $Ca_2Mn^{2+}Re^{6+}O_6$ and $Ca_2Mn^{3+}Re^{5+}O_6$.

For each valence case (Mn^{2+} and Mn^{3+} configurations) there are two possibilities of spin state configurations for the cations: the low-spin state and the high-spin state. These states arise from the split of crystalline field in transition metal coordination complexes due to the competition between exchange force and crystalline electric field, just like the octahedral field in double perovskite compounds. The main implication for the whole system concerns magnetic properties, but there are some structural consequences. From Shannon's table [35] we can see that the difference between the ionic radii in Mn^{3+}, for example, lies in 10% (64.5 pm for the high spin configuration and 58 pm for the low one). In double perokskite compounds, the B' site is usually occupied by a magnetic atom, for B' = Mn^{2+} the exchange split is about 4 eV [36]. The high spin configuration is due to the crystalline field energy ~ 1 eV, and occurs in most of the cases. On the contrary, the B'' site is occupied by a non-magnetic atom and the exchange coupling is negligible, thus the low spin state prevails.

In summary, taking into account the comparative analysis of the parameters shown in Tables I, II and III, it is not possible to determine the exact cation valence configuration ($Mn^{2+}Re^{6+}$ or $Mn^{3+}Re^{5+}$) for this $Ca_2Mn_1Re_1O_6$ structural monophasic compound. Magnetic measurements can bring more information about this double perovskite. However, in our point of view, the XANES analysis can complete description of local Mn-O and Re-O configuration. In order to investigate the valence of Mn and Re in $Ca_2Mn_1Re_1O_6$, X-ray absorption experiments were done.

X ray absorption spectroscopy

Information about the average oxidation state of Mn and Re and the local structural distortion around these ions are provided by X-ray absorption spectroscopic investigation. The valence configuration of the atoms is commonly determined by the chemical shift of the atomic absorption edge to high energy. Fig. 4 shows the Mn-K edge of the ordered double perovskite compound $Ca_2Mn_1Re_1O_6$ along with the MnO (Mn^{2+}), Mn_2O_3 (Mn^{3+}), MnO_2 (Mn^{4+}) and $KMnO_4$ (Mn^{6+}) standards. Clearly, the proximity of the main Mn edge of the $Ca_2Mn_1Re_1O_6$ perovskite to that of MnO standard near the absorption coefficient $\mu = 1$ (the box in Fig. 4) is consistent with a $Mn^{+2.3}$ assignment. In addition, the features indicated by the arrows suggest that the coordination of the Mn atom in double perovskite is rather similar to that of MnO standard.

Fig. 5 shows the Re-L_{III} edge for the $Ca_2Mn_1Re_1O_6$ perovskite along with the ReO_3 (Re^{6+}) and ReO_2 (Re^{5+}) standards. One may notice the splitting of the white-line feature in transition metals due to transitions into final *d* states, namely e_g/t_{2g} states (A-B features in Fig. 5). The coincidence of position of the Re-L_{III} edge of the double

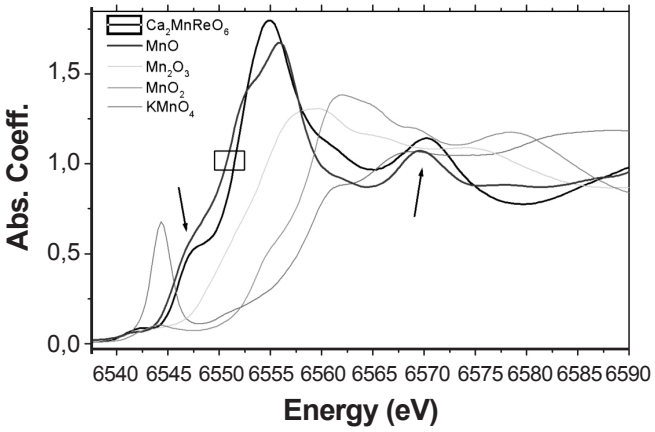

Figure 4: Mn-K edge of compound $Ca_2Mn_1Re_1O_6$ with the standards. The box near the $\mu = 1$ and the arrows indicate the proximity of MnO configuration.

[Figura 4: Borda K de absorção do Mn no composto $Ca_2Mn_1Re_1O_6$ com os padrões. A caixa próxima de $\mu = 1$ e as setas indicam a semelhança do $Ca_2Mn_1Re_1O_6$ com a configuração MnO.]

perovskite and that of ReO_3 suggests an approximate Re^{6+} state. A quantitative analysis may be taken if one uses the first moment (E_m) of the white-line feature (defined below) in order to estimate the chemical shift:

$$Em = \left[\int_{E_L}^{E_H} E\mu\,(E)\,dE\right]\left[\int_{E_L}^{E_H} \mu\,(E)\,dE\right]^{-1}$$

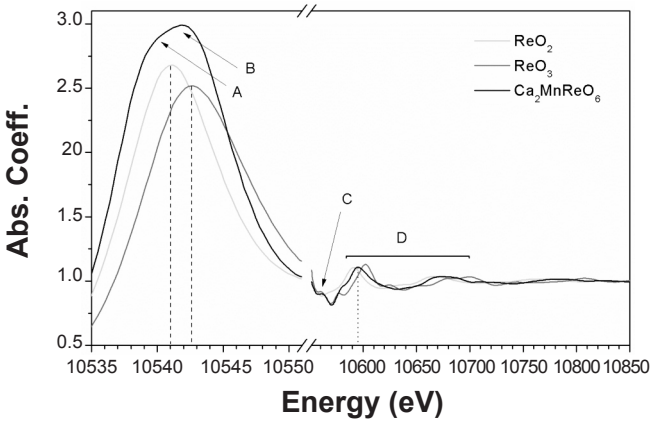

Figure 5: Re-L3 edge of the compound $Ca_2Mn_1Re_1O_6$ ploted with the standards.

[Figura 5: Borda L_{III} do Rênio no composto $Ca_2Mn_1Re_1O_6$. desenhada em conjunto com os padrões de comparação.]

This method was used for the first time by Alp *et al.* [37] to define de Cu valence and charge transfer effect. Popov *et al.* [22] also have applied such method to study the valence of Mn and Re ions in a MnRe-based double perovskite series, just like in our case. The point to be considered here is the choice of the high-low energy limits in the integrals. The low-energy limit E_L is insensitive to the cutoff since the

background pre-edge subtraction process results in $\mu \sim 0$ in this range, so it was chosen to be 100 eV below the edge in order to encompass the entire white-line feature. The high-energy cutoff was chosen to take into account the majority of the white-line feature weight but not so high to capture the EXAFS range ($\mu \sim 1.0$). Accordingly, we have fixed the high-energy limit to have μ (E_H) = 1.4. Taking as a reference the E_m values of the standards, it was found a fitting point +5.7 to a valence of the Re ions in $Ca_2Mn_1Re_1O_6$ double perovskite compound. The coordination feature indicated by the C features in Fig. 5 agrees with the similar symmetry of Re ion (D_{4h}) in ReO_3 standard. The region D of Fig. 5 may be regarded as a region of local environment information, and it is well known that the prominent peak moves to higher energies with decreasing the Re-O bond lengths. Thereby, in D-feature of Fig. 5 the position of perovskite peak is consistent with the result of intermediate valence between Re^{4+} (ReO_2) and Re^{6+} (ReO_3) for Re ion.

CONCLUSIONS

A structural monophasic Ca_2MnReO_6 double perovskite oxide was synthesized from a mixture of CaO, MnO_2, ReO_2 and ReO_3 powders in the nominal stoichiometric ratio 2:1:0.9:0.1 using the encapsulated quartz tube technique. The 0.9:0.1 ratio between ReO_2 and ReO_3 was used to guarantee a partial pressure of oxygen inside the quartz tube at high temperatures. This partial pressure of oxygen was revealed to be a crucial synthesis parameter for the production of a single phase sample. The filling factor parameter was set to $ff \cong 0.12$ g/cm^3 in order to obtain a partial pressure of 3 bar inside the tube at high temperatures for the first thermal treatment. The EDS analysis confirmed that the product only contains the elements Ca, Mn, Re, and O, and the electron backscattered SEM images indicated an homogenous chemical compositon corresponding to the Ca_2MnReO_6 double perovskite oxide. The Rietveld refinement indicated a monoclinic unit cell with rock-salt order of the Mn and Re ions, space group $P\,2_1/n$, with a = 5.44445(2) Å; b = 5.63957(3) Å; c = 7.77524(3) Å and β = 90.18(1)º, and show low Re/Mn cationic disorder (~ 3%). The Rietveld refinement also reveals there is only one structural phase. The *SPuDS* program simulation proposes two possible cation valence configurations, namely, (i) $Mn^{2+}Re^{6+}$ or (ii) $Mn^{3+}Re^{5+}$, for the $Ca_2Mn_1Re_1O_6$ compound. XANES measurements indicated +2.3 for the average valence of Mn (a mixture of Mn^{2+} and Mn^{3+}) and +5.7 for the effective valence of Re (an intermediate valence between Re^{4+} (ReO_2) and Re^{6+} (ReO_3)).

As a summary, based on our experiments, we concluded there is a mixed valence configuration for Mn and Re in $Ca_2Mn_1Re_1O_6$, taking into account the oxygen content of 6.0±0.1. We suggest that some magnetic measurements are necessary for a complete description of this behavior.

ACKNOWLEDGEMENTS

We would like to thank the Brazilian agencies grants: CNPq CT-Energ 504578/2004-9, CNPq 471536/2004-0, CNPq 480337/2007-1 and CAPES for financial support. Thanks are also due to Companhia Siderurgica de Tubarão (ArcelorMittal). We gratefully acknowledge the Brazilian National Synchrotron Light Laboratory - LNLS (XPD and XAS measurements).

REFERENCES

[1] J. Longo, R. Ward, J. Am. Chem. Soc. **83** (1961) 2816.
[2] A. W. Sleight, J. Longo, R. Ward, Inorg. Chem. **1** (1962) 245.
[3] J. M. D. Coey, M. Viret, S. von Molnar, Adv. Phys. **48** (1999) 167.
[4] S. A. Wolf, D. D. Awschalom, R. A. Buhram, J. M. Daughton, S. von Molnár, M. L. Roukes, A. Y. Chtchelkanova, D. M. Treger, Science **294** (2001) 1488.
[5] S. A. Wolf, A. Y. Chtchelkanova, D. M. Treger, IBM J. Res. Dev. **50**, 1 (2006).
[6] S. Parkin, X. Jiang, C. Kaiser, A. Panchula, K. Roche, M. Samant, Proc. IEEE **91**, 5 (2003).
[7] P. Foldi, O. Kalman, M. G. Benedict, F. M. Peeters, Nano Lett. **8** (2008) 2556.
[8] M. N. Leuenberg, M. E. Flatté, D. D. Awschalom, Phys. Rev. Lett. **94** (2005) 107401.
[9] S. D. Sarma, J. Fabian, X. Hu, I. Zutic, Solid State Comm. **119** (2001) 207.
[10] C.-Y. You, S. D. Bader, J. Appl. Phys. **87** (2000) 5215.
[11] H. Dery, L. J. Sham, Phys. Rev. Lett. **98** (2007) 046602.
[12] A. Quesada, M. A. García, J. de La Venta, E. F. Pinel, J. M. Merino, A. Hernando, Eur. Phys. J. B **59** (2007) 457.
[13] K.-I. Kobayashi, T. Kimura, H. Sawada, K. Terakura, Y. Tokura, Nature **395** (1998) 677.
[14] Z. Zeng, I. D. Fawcett, M. Greenblatt, M. Croft, Mater. Res. Bull. **36** (2001) 705.
[15] Z. Fang, K. Terakura, J. Kanamori, Phys. Rev. B **63** (2001) 180507(R).
[16] G. Popov, M. V. Lobanov, E. V. Tsiper, M. Greenblatt, E. N. Caspi, A. Borissov, V. Kiryukhin, J. W. Lynn, J. Phys.: Cond. Matt. **16** (2004) 135.
[17] H. Kato, T. Okuda, Y. Okimoto, Y. Tomioka, K. Oikawa, T. Kamiyama, Y. Tokura, Phys. Rev. B **69** (2004) 184412.
[18] J. B. Philipp, P. Majewski, L. Alff, A. Erb, R. Gross, T. Graf, M. S. Brant, J. Simon, T. Walther, W. Mader, D. Topwal, D. D. Sarma, Phys. Rev. B **68** (2003) 144431.
[19] M. W. Lufaso, P. W. Barnes, P. M. Woodward, Acta Cryst. B**62** (2006) 397.
[20] D. Serrate, J. M. De Teresa, M. R. Ibarra, J. Phys.: Cond. Matt. **19** (2007) 023201.
[21] M. W. Lufaso, P. M. Woodward, Acta Crystallogr., Sect. B: Struct. Sci. **57** (2001) 725.
[22] G. Popov, M. Greenblatt, M. Croft, Phys. Rev. B **67** (2003) 024406.
[23] E. Granado, Q. Huang, J. W. Lynn, J. Gopalakrishnan, R. L. Grenee, K. Ramesha, Phys. Rev. B **66** (2002) 064409.
[24] J. Herrero-Martín, G. Subías, J. Blasco, J. García, M. C. Sánchez, J. Phys.: Cond. Matt. **17** (2005) 4963.

[25] M. Sikora, Cz. Kapusta, M. Borowiec, C. J. Oates, V. Prochazka, D. Rybicki, D. Zajac, J. M. De Teresa, C. Marquina, M. R. Ibarra, Appl. Phys. Lett. **89** (2005) 062509.
[26] J. M. Michalik, J. M. De Teresa, J. Blasco, P. A. Algarabel, M. R. Ibarra, Cz Kapusta, U. Zeitler J. Phys.: Condens. Matter **19** (2007) 506206.
[27] A. C. Larson, B. Von Dreele, General Structure Analysis System (GSAS), Report LAUR 86-748, Los Alamos, N. Mex., USA (2000).
[28] H. B. Toby, J. Appl. Crystallog. **4** (2001) 210.
[29] P. Thompson, D. E. Cox, J. B. Hastings, J. Appl. Crystallog. **20** (1987) 79.
[30] L. W. Finger, D. E. Cox, A. P. Jephcoat, J. Appl. Crystallog. **27** (1994) 890.
[31] P. W. Stephens, J. Appl. Crystallog. **32** (1999) 281.
[32] A. M. Glazer, Acta Crystallogr. B **28** (1972) 3384.
[33] I. D. Brown, *in* M. O'Keefe, A. Navrotsky (Eds.): Structure and Bonding in Crystals, Vol **2**, p. 1, Academic Press, New York (1981).
[34] N. E. Brese, M. O'Keefe, Acta Crystallogr. B **47** (1991) 192.
[35] R. D. Shannon, Acta Crystallogr. A **32** (1976) 751.
[36] H. Wu, Phys. Rev. B **64** (2001) 125126.
[37] E. E. Alp, G. L. Goodman, L. Soderholm, S. M. Mini, M. Ramanathan, G. K. Shenoy, A. S. Bommannavar, J. Phys.: Condensed Matter. **1** (1989) 6463.
(Rec. 28/07/2009, Rev. 12/01/2010, Ac. 14/01/2010)